

# **$^1\text{H}$ , $^{13}\text{C}$ , $^{15}\text{N}$ resonance assignment of the *apo* form of the small, chitin-active lytic polysaccharide monoxygenase *JdLPMO10A* from *Jonesia denitrificans***

Idd A. Christensen<sup>1</sup>, Vincent G. H. Eijsink<sup>2</sup>, Finn L. Aachmann<sup>1</sup>, Gaston Courtade<sup>1,\*</sup>

## ORCIDs

Idd A. Christensen: 0000-0001-6229-2211

Vincent G. H. Eijsink: 0000-0002-9220-8743

Finn L. Aachmann: 0000-0003-1613-4663

Gaston Courtade: 0000-0002-1644-3223

<sup>1</sup>NOBIPOL, Department of Biotechnology and Food Science, NTNU Norwegian University of Science and Technology, Sem Sælands vei 6/8, N-7491 Trondheim, Norway.

<sup>2</sup>Faculty of Chemistry, Biotechnology and Food Science, NMBU Norwegian University of Life Sciences, N-1432 Ås, Norway.

\*To whom correspondence should be addressed: [gaston.courtade@ntnu.no](mailto:gaston.courtade@ntnu.no)

## **Abstract:**

The lytic polysaccharide monoxygenase *JdLPMO10A* is the N-terminal domain of the multimodular protein *Jd1381*. The isolated *JdLPMO10A* domain is one of the smallest chitin-active lytic polysaccharide monoxygenases known to date with a size of only 15.5 kDa. *JdLPMO10A* is a copper-dependent oxidative enzyme that depolymerizes chitin by hydroxylating the C1 carbon in the glycosidic bond. *JdLPMO10A* has been isotopically labeled and recombinantly expressed. Here, we report the  $^1\text{H}$ ,  $^{13}\text{C}$ ,  $^{15}\text{N}$  resonance assignment of *JdLPMO10A*. Secondary structural elements predicted based on the NMR assignment are in excellent agreement with the crystal structure of *JdLPMO10A*.

## **Keywords:**

Lytic polysaccharide monoxygenase (LPMO), chitin

## **Biological context:**

Lytic polysaccharide monoxygenases (LPMOs) are a family of copper-dependent oxidative enzymes that cleave  $\beta(1,4)$ -glycosidic bonds in recalcitrant polysaccharides such as cellulose and chitin (Vaaje-Kolstad et al. 2005, 2010; Quinlan et al. 2011; Hemsworth et al. 2015; Forsberg et al. 2019). LPMOs boost the degradation of crystalline polysaccharides by creating free polysaccharide chain ends that canonical glycoside hydrolases (GHs) can act on. Understanding LPMO function is therefore of interest for the biorefinery concept and may

prove instrumental to achieve cost-effective saccharification of polysaccharides needed to subsequently produce biomaterials, platform chemicals and biofuels (Beeson et al. 2015).

LPMOs are classified in the Auxiliary Activity (AA) families AA9-AA11 and AA13-AA16 in the Carbohydrate Active Enzymes (CAZy) database (Levasseur et al. 2013). LPMOs are copper-dependent redox enzymes that hydroxylate scissile glycosidic bonds, thus destabilizing this bond and causing cleavage (Quinlan et al. 2011; Beeson et al. 2012; Agger et al. 2014; Chylenski et al. 2019). While cellulose-active LPMOs oxidize either the C1 or C4 position, or both, only C1 oxidation has been demonstrated for chitin-active LPMOs so far. LPMOs were initially believed to catalyze a monooxygenase, i.e. an oxygen-dependent, reaction (Vaaje-Kolstad et al. 2010), but recent findings indicate that H<sub>2</sub>O<sub>2</sub> might be the true co-substrate of LPMOs (Bissaro et al. 2017). The reaction mechanism of LPMOs remains to be uncovered in detail and is the subject of ongoing research (Chylenski et al. 2019; Courtade et al. 2020; Jones et al. 2020)

*JdLPMO10A* is a small C1-oxidizing chitin-active LPMO with a size of 15.5 kDa (Mekasha et al. 2016). In nature, *JdLPMO10A* is found as the N-terminal domain of the larger multi-domain protein *Jd1381*. *Jd1381* is secreted when the Gram-positive bacterium *Jonesia denitrificans* grows on chitin and might be the only chitinase produced by *J. denitrificans*, known to degrade both  $\alpha$ - and  $\beta$ -chitin (Mekasha et al. 2020). *JdLPMO10A* can cleave both allomorphs of chitin through a C1-mediated mechanism (Mekasha et al., 2016).

The structure of *JdLPMO10A* has been determined using X-ray crystallography (Mekasha et al., 2016; PDB accession number: 5AA7). Like all LPMOs, *JdLPMO10A* has a  $\beta$ -sandwich core made up of seven  $\beta$ -strands that are connected through a series of loops. In the copper active site, located on the enzyme's substrate-binding surface, a single copper ion is coordinated by the amino group of the N-terminal His, the side-chain (N <sup>$\delta$ 1</sup>) of the same residue, and the side-chain (N <sup>$\epsilon$ 2</sup>) of His78, in a motif referred to as the histidine brace (Quinlan et al. 2011; Mekasha et al. 2016). In addition to the crystal structure, a neutron structure of *JdLPMO10A* is also available (Bacik et al. 2017).

*JdLPMO10A* with a size of 15.5 kDa (142 amino acids) represents one of the smallest LPMOs known to date. NMR has successfully been used to characterize the structure of the copper-free *apo*- form of several bacterial (Aachmann et al. 2012; Courtade et al. 2015, 2016,

2018) and one fungal LPMO in the past (Kitaoku et al. 2018).

The *apo*-form is preferred to avoid loss of signal caused by paramagnetic relaxation enhancement effects that would result from the presence of a type II copper site (Bertini and Pierattelli 2004). It has previously been shown that the absence of copper has a minimal effect on the 3-dimensional structure of LPMOs, affecting only the orientations of two histidine residues in the copper-active site (Aachmann et al. 2012; Courtade et al. 2020). Investigating *apo*-*JdLPMO10A* can therefore provide an understanding of the LPMO core structure which might in turn provide valuable insight that can be used for future optimization of LPMO function.

### **Methods and experiments:**

The NMR assignment was performed on the recombinantly expressed *apo* form of *JdLPMO10A*. The gene encoding *JdLPMO10A* (UniProt ID C7R4I0, residues 32-173) includes a 31-residue long N-terminal residue signal peptide (Mekasha et al. 2016). In *E. coli*, the signal peptide is cleaved during the process of periplasmic translocation, resulting in the accumulation of mature LPMO, with the desired N-terminal His, in the periplasm in the cell.

Cloning, expression, and purification were performed as described by Courtade *et al.* (Courtade et al. 2017), with minor modifications. *E. coli* strain T7 express (New England Biolabs) was used for cloning. Pre-cultures of 25 mL Lysogeny Broth (LB) medium (10 g/L tryptone, 5 g/L yeast extract, 5 g/L NaCl) with 100 µg/mL ampicillin were inoculated with transformed *E. coli* T7 express cells and incubated at 30 °C and 225 RPM overnight. To obtain isotopically labeled samples (<sup>15</sup>N and <sup>13</sup>C/<sup>15</sup>N), cells were grown in 500 mL M9 medium (6 g/L Na<sub>2</sub>HPO<sub>4</sub>, 3g/L KH<sub>2</sub>PO<sub>4</sub>, 0.5 g/L NaCl) with 1 g/L (<sup>15</sup>NH<sub>4</sub>)<sub>2</sub>SO<sub>4</sub>, trace metal solution, MEM vitamin solution (Thermo Fisher Scientific), Bioexpress cell growth medium (10x, either <sup>15</sup>N or <sup>13</sup>C/<sup>15</sup>N-labeled), 2 g/L <sup>13</sup>C-D-glucose (for <sup>13</sup>C/<sup>15</sup>N-labeled sample only) or D-glucose (for <sup>15</sup>N-labeled sample), and 100 µg/mL ampicillin. All isotopically enriched medium components were purchased from Cambridge Isotope Laboratories. The 500 mL cultures were inoculated with 1 % (v/v) of pre-culture and incubated at 30 °C and 225 RPM until an OD<sub>600</sub> ~ 0.8-1.2 was obtained. The cultures were then cooled on ice for 5 minutes before being induced by adding m-toluic acid to a final concentration of 100 µM. The induced cultures were incubated overnight at 16 °C and 225 RPM.

*JdLPMO10A* was extracted from the periplasmic space using an osmotic shock method (Nossal and Heppel 1966). The cells were harvested by centrifugation at 4000 xg and 4 °C for 10 minutes. The supernatant was discarded and the cell pellet was incubated on ice for 5 minutes prior to resuspension in ice-cold 30 mL spheroplast buffer (100 mM Tris-HCl, pH 8.0, 0.5 M sucrose, 0.5 mM EDTA) supplemented with half of a cOmplete™ ultra protease inhibitor tablet (Roche). After 5 minutes incubation on ice, the resuspended cells were centrifuged at 5000 xg and 4 °C for 10 minutes and the supernatant was discarded. The cell pellet was incubated at room temperature for 10 minutes and then resuspended in 25 mL ice-cold ultrapure water with half of a cOmplete™ ultra protease inhibitor tablet. After 45 seconds, 1.5 mL of 20 mM MgCl<sub>2</sub> was added to the resuspended cells, followed by centrifugation at 15000 xg and 4 °C for 15 minutes. The supernatant, containing the periplasmic extract, was kept and filtered through a 0.22 µm filter, prior to storage at 4 °C.

*JdLPMO10A* was purified using a weak anion-exchange column (5 mL, HiTrap DEAF FF, GE Healthcare and Life Sciences) coupled to an ÄKTASTART automatic liquid chromatography system (GE Healthcare and Life Sciences). The column was first equilibrated with 5 column volumes (CV) sterile-filtered ultrapure water and then equilibrated with 5 CV of sterile-filtered equilibration buffer (50 mM Tris-HCl, pH 8.0). The periplasmic extract was loaded onto the column and unbound proteins were removed by washing the column with an additional 5 CV of equilibration buffer. The bound proteins were eluted from the column by applying a linear salt gradient where the fraction of sterile-filtered elution buffer (50 mM Tris-HCl, 1 M NaCl, pH 8.0) was increased from 0 to 50 % over a total volume of 60 CV. The protein eluted from the column at 12% elution buffer. The flow rate was kept constant at 4.5 mL/min throughout the experiment.

Fractions containing *JdLPMO10A* were identified by SDS-PAGE, pooled, and concentrated by spinning down to a volume of < 5 mL using VivaSpinn columns (10 kDa cut-off, Sartorius). Size Exclusion Chromatography (SEC) with a 100 mL HiLoad® 16/600 Superdex® G-75 pg column was used to further purify the concentrated protein solution. The column was equilibrated with 3 CV of ultrapure water, followed by 3 CV of sterile-filtered SEC buffer (25 mM Tris-HCl, 250 mM NaCl, pH 8.0). The sample was loaded onto the column with a flow rate of 1 mL/min. Fractions containing *JdLPMO10A* eluted at about 60 mL after injection. Fractions containing *JdLPMO10A* (purity assessed by SDS-PAGE) were

pooled, and the buffer was changed to the buffer used for NMR data collection (20 mM NaH<sub>2</sub>PO<sub>4</sub>, 10 mM NaCl, pH 5.5) with 10% D<sub>2</sub>O (d-99.9%, Sigma-Aldrich). In order to minimize the water signal in <sup>13</sup>C-HSQC, HcCH-TOSCY and <sup>13</sup>C-NOESY-HSQC spectra (see below), the <sup>13</sup>C/<sup>15</sup>N-labeled sample buffer was later changed to the NMR buffer with 99.9% D<sub>2</sub>O. NMR samples of 160 μL were prepared in 3 mm tubes with a concentration of 200 μM protein. Three samples of *JdLPMO10A* were produced in total, one <sup>15</sup>N-labeled sample, and two <sup>13</sup>C/<sup>15</sup>N-labeled samples. The latter were pooled to one NMR sample. No copper was added to the NMR samples meaning all NMR data were acquired on *apo-JdLPMO10A*.

All the NMR spectra were recorded at 25 °C using a Bruker Avance III HD 800 MHz spectrometer equipped with a 5-mm Z-gradient CP-TCI (H/C/N) cryogenic probe at the NV-NMR-Centre/Norwegian NMR Platform (NNP) at the Norwegian University of Science and Technology (NTNU). <sup>1</sup>H chemical shifts were internally referenced to the water signal, while <sup>15</sup>N and <sup>13</sup>C chemical shifts were indirectly referenced to the water signal, based on absolute frequency ratios (Zhang et al. 2003). Sequence-specific backbone and side-chain assignments were accomplished using <sup>15</sup>N-HSQC, <sup>13</sup>C-HSQC, HNCA, HNcoCA, HNCOC, HNCaCO, HNCACB, HNcoCACB, HcCH-TOSCY, <sup>15</sup>N- NOESY- HSQC, and <sup>13</sup>C- NOESY-HSQC. All spectra were processed using TopSpin version 3.5.7. Spectra were analyzed in CARA (Computer Aided Resonance Assignment) version 1.8.4 (Keller 2004). Secondary structural elements were predicted based on the NMR data using TALOS-N (Shen and Bax 2013) using the N, H<sup>N</sup>, C<sup>α</sup>, C<sup>β</sup>, H<sup>α</sup>, H<sup>β</sup>, C' chemical shifts as the input. The φ and ψ dihedral angles predicted by TALOS-N were compared with the corresponding angles from the X-ray crystal diffraction structure (Mekasha et al., 2016; PDB accession number: 5AA7).

### **Extent of assignment and data deposition**

Here we report the backbone and side-chain resonance assignment of the lytic polysaccharide monoxygenase *JdLPMO10A*. The <sup>15</sup>N-HSQC spectrum of *JdLPMO10A* with the assigned resonances is shown in Figure 1. The backbone assignment is almost complete (H<sup>N</sup>, H<sup>α</sup>, N, C<sup>α</sup>, C' > 90%), assigned residues are shown in Figure 2. Side-chains were partially assigned (H and C side-chains ~ 43.5%). None of the exchangeable side-chain protons of Arg, Lys, Asn and Gln or aromatic residues were assigned. The NH-group of the N-terminal histidine was not assigned. The chemical shifts have been deposited in the Biological Magnetic Resonance Data Bank (BMRB) under the accession number 50338.

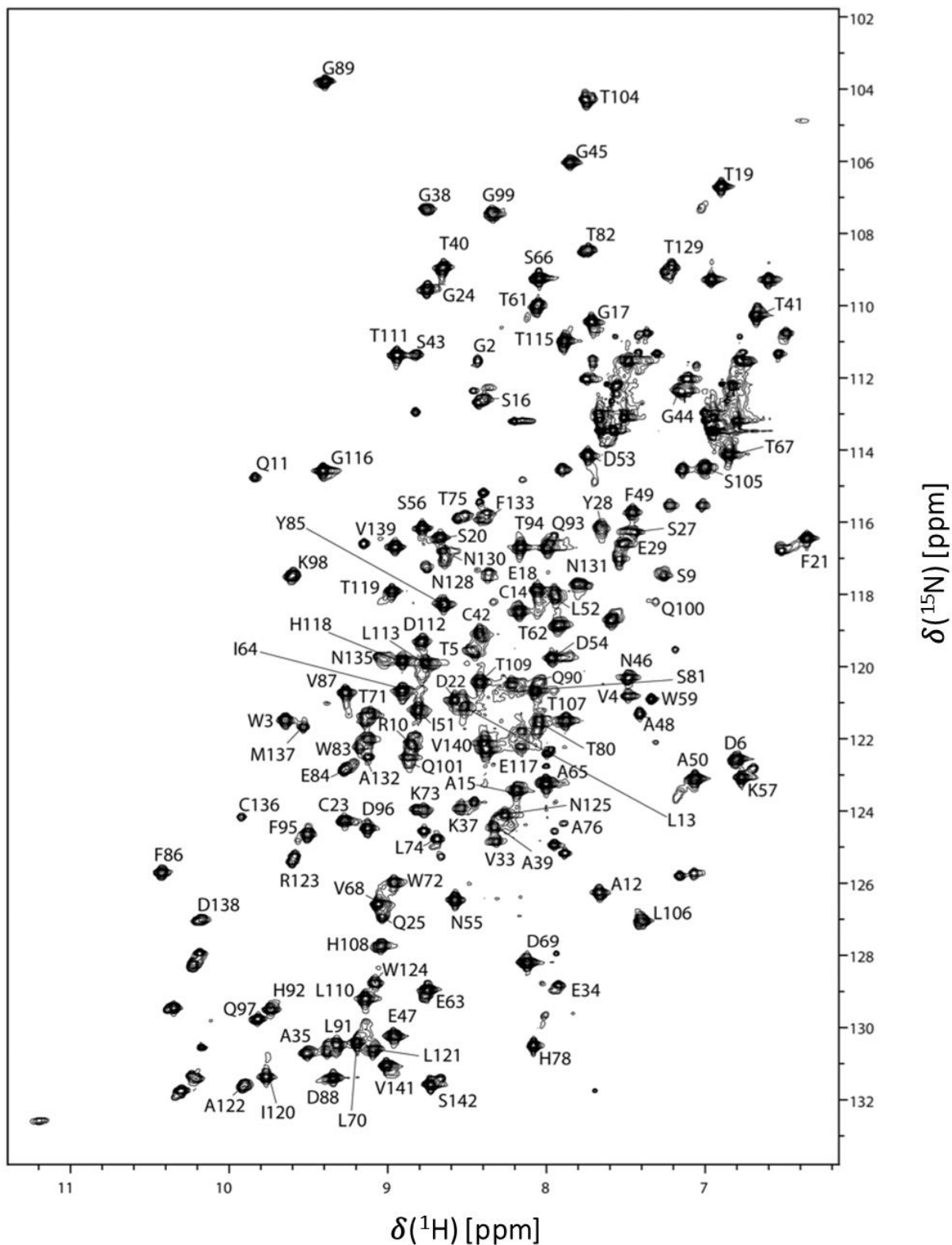


Figure 1:  $^1\text{H}$ - $^{15}\text{N}$  HSQC spectrum of  $^{13}\text{C}/^{15}\text{N}$ -isotopically labeled *JdLPMO10A* from the Gram-positive bacterium *Jonesia denitrificans* in sodium phosphate buffer, pH 5.5, with 10 mM NaCl, in 90%  $\text{H}_2\text{O}/10\%$   $\text{D}_2\text{O}$ . Residue number and type are indicated in the figure.

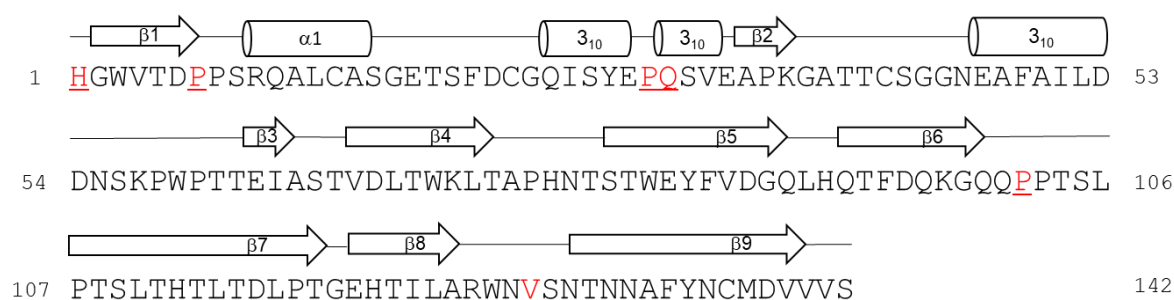


Figure 2: Overview of the chemical shift assignment of the backbone of *JdLPMO10A* ( $H^N$ ,  $H^\alpha$ , N,  $C^\alpha$ ,  $C'$  > 90%). Assigned residues are shown in black while residues without assigned chemical shifts are shown in red. The secondary structural elements of *JdLPMO10A* are placed above the corresponding segments of the primary structure.

Dihedral angles predicted by TALOS-N based on the chemical shift assignment are in excellent agreement with the published crystal structure of *JdLPMO10A* (Mekasha et al. 2016; PDB accession number: 5AA7), as shown in Figure 3. The differences in the torsion angles observed for the N-terminal residues are mainly the result of missing chemical shift assignments. In the absence of chemical shifts, TALOS-N predicts the torsion angles based on the primary sequence of the protein (Shen and Bax 2015) making the prediction less reliable.

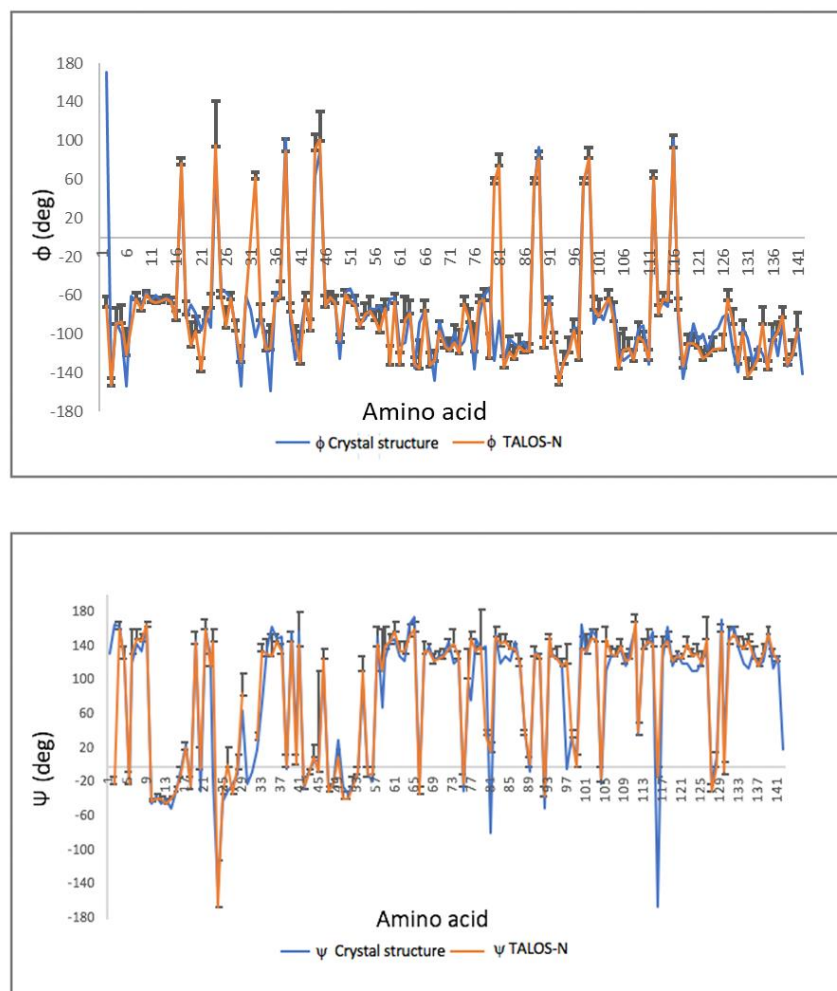


Figure 3: Comparison of the dihedral angles phi ( $\phi$ ) and psi ( $\psi$ ) obtained for *JdLPMO10A* using TALOS-N (based on chemical shifts determined by NMR) and X-ray crystallography (Mekasha et al. 2016; PDB ID 5AA7) plotted against amino acid residue number. The dihedral angles determined using TALOS-N are presented together with the corresponding standard deviation for each residue.

We have presented the  $^1\text{H}$ ,  $^{13}\text{C}$ ,  $^{15}\text{N}$  resonance assignment of the LPMO *JdLPMO10A*. The assignment will allow for functional investigations of this minimal LPMO structure using NMR spectroscopy. Future areas of interest include studying the interactions between *JdLPMO10A* and chitin, as well as the interplay with other redox-active enzymes. Increased understanding of LPMOs may pave the way for improving the biocatalytic conversion of biomass.

### **Acknowledgements:**

This work was financed by the Novo Nordisk Foundation (grant number NNF18OC0032242), the OXYMOD project, the Norwegian NMR Platform and a FRIPRO project (grants 269408, 226244 and 262853 from the Research Council of Norway, respectively).

### **Conflict of interest:**

The authors declare that they have no conflict of interest.

### **References**

- Aachmann FL, Sørli M, Skjåk-Bræk G, et al (2012) NMR structure of a lytic polysaccharide monooxygenase provides insight into copper binding, protein dynamics, and substrate interactions. *Proc Natl Acad Sci* 109:18779–18784.  
<https://doi.org/10.1073/PNAS.1208822109>
- Agger JW, Isaksen T, Várnai A, et al (2014) Discovery of LPMO activity on hemicelluloses shows the importance of oxidative processes in plant cell wall degradation. *Proc Natl Acad Sci U S A* 111:6287–6292. <https://doi.org/10.1073/pnas.1323629111>
- Bacik JP, Mekasha S, Forsberg Z, et al (2017) Neutron and atomic resolution X-ray structures of a lytic polysaccharide monooxygenase reveal copper-mediated dioxygen binding and evidence for N-terminal deprotonation. *Biochemistry* 56:2529–2532.  
<https://doi.org/10.1021/acs.biochem.7b00019>
- Beeson WT, Phillips CM, Cate JHD, Marletta MA (2012) Oxidative cleavage of cellulose by fungal copper-dependent polysaccharide monooxygenases. *J Am Chem Soc* 134:890–892. <https://doi.org/10.1021/ja210657t>
- Beeson WT, Vu V V, Span EA, et al (2015) Cellulose degradation by polysaccharide monooxygenases. *Annu Rev Biochem* 84:923–946. <https://doi.org/10.1146/annurev-biochem-060614-034439>
- Bertini I, Pierattelli R (2004) Copper(II) proteins are amenable for NMR investigations. *Pure Appl Chem* 76: 321–333. <https://doi.org/10.1351/pac200476020321>
- Bissaro B, Røhr ÅK, Müller G, et al (2017) Oxidative cleavage of polysaccharides by monocopper enzymes depends on H<sub>2</sub>O<sub>2</sub>. *Nat Chem Biol* 13:1123–1128.  
<https://doi.org/10.1038/nchembio.2470>
- Chylenski P, Bissaro B, Sørli M, et al (2019) Lytic polysaccharide monooxygenases in enzymatic processing of lignocellulosic biomass. *ACS Catal* 9:4970–4991.  
<https://doi.org/10.1021/acscatal.9b00246>

- Courtade G, Ciano L, Paradisi A, et al (2020) Mechanistic basis of substrate–O<sub>2</sub> coupling within a chitin-active lytic polysaccharide monooxygenase: An integrated NMR/EPR study. *Proc Natl Acad Sci*. 117:19178-19189. <https://doi.org/10.1073/pnas.2004277117>
- Courtade G, Forsberg Z, Heggset EB, et al (2018) The carbohydrate-binding module and linker of a modular lytic polysaccharide monooxygenase promote localized cellulose oxidation. *J Biol Chem* 293:13006–13015. <https://doi.org/10.1074/jbc.RA118.004269>
- Courtade G, Le SB, Sætrom GI, et al (2017) A novel expression system for lytic polysaccharide monooxygenases. *Carbohydr Res* 448:212–219. <https://doi.org/10.1016/j.carres.2017.02.003>
- Courtade G, Wimmer R, Dimarogona M, et al (2016) Backbone and side-chain <sup>1</sup>H, <sup>13</sup>C, and <sup>15</sup>N chemical shift assignments for the apo-form of the lytic polysaccharide monooxygenase NcLPMO9C. *Biomol NMR Assign* 10:277-280. <https://doi.org/10.1007/s12104-016-9683-x>
- Courtade G, Balzer S, Forsberg Z, et al (2015) <sup>1</sup>H, <sup>13</sup>C, <sup>15</sup>N resonance assignment of the chitin-active lytic polysaccharide monooxygenase BILPMO10A from *Bacillus licheniformis*. *Biomol NMR Assign* 9:207–210. <https://doi.org/10.1007/s12104-014-9575-x>
- Forsberg Z, Sørli M, Petrović D, et al (2019) Polysaccharide degradation by lytic polysaccharide monooxygenases. *Curr Opin Struct Biol* 59:54–64. <https://doi.org/10.1016/j.sbi.2019.02.015>
- Hemsworth GR, Johnston EM, Davies GJ, Walton PH (2015) Lytic polysaccharide monooxygenases in biomass conversion. *Trends Biotechnol* 33:747–761. <https://doi.org/10.1016/j.tibtech.2015.09.006>
- Jones SM, Transue WJ, Meier KK, et al (2020) Kinetic analysis of amino acid radicals formed in H<sub>2</sub>O<sub>2</sub>-driven CuI LPMO reoxidation implicates dominant homolytic reactivity. *Proc Natl Acad Sci U S A* 117:11916–11922. <https://doi.org/10.1073/pnas.1922499117>
- Keller R (2004) The computer aided resonance assignment tutorial. CANTINA Verlag, Goldau
- Kitaoku Y, Courtade G, Petrović DM, et al (2018) Resonance assignments for the apo-form of the cellulose-active lytic polysaccharide monooxygenase TaLPMO9A. *Biomol NMR Assign* 12:357–361. <https://doi.org/10.1007/s12104-018-9839-y>
- Levasseur A, Drula E, Lombard V, et al (2013) Expansion of the enzymatic repertoire of the CAZy database to integrate auxiliary redox enzymes. *Biotechnol Biofuels* 6:41. <https://doi.org/10.1186/1754-6834-6-41>

- Mekasha S, Forsberg Z, Dalhus B, et al (2016) Structural and functional characterization of a small chitin-active lytic polysaccharide monooxygenase domain of a multi-modular chitinase from *Jonesia denitrificans*. FEBS Lett 590:34–42.  
<https://doi.org/10.1002/1873-3468.12025>
- Mekasha S, Tuveng TR, Askarian F, et al (2020) A tri-modular bacterial enzyme combining hydrolytic activity with oxidative glycosidic bond cleavage efficiently degrades chitin. J Biol Chem. <https://doi.org/10.1074/jbc.RA120.013040>
- Nossal NG, Heppel LA (1966) The release of enzymes by osmotic shock from *Escherichia coli* in exponential phase. J Biol Chem 241:3055–3062
- Quinlan RJ, Sweeney MD, Lo Leggio L, et al (2011) Insights into the oxidative degradation of cellulose by a copper metalloenzyme that exploits biomass components. Proc Natl Acad Sci U S A 108:15079–15084. <https://doi.org/10.1073/pnas.1105776108>
- Shen Y, Bax A (2015) Protein structural information derived from nmr chemical shift with the neural network program TALOS-N. Methods Mol Biol 1260:17–32.  
[https://doi.org/10.1007/978-1-4939-2239-0\\_2](https://doi.org/10.1007/978-1-4939-2239-0_2)
- Shen Y, Bax A (2013) Protein backbone and sidechain torsion angles predicted from NMR chemical shifts using artificial neural networks. J Biomol NMR 56:227–241.  
<https://doi.org/10.1007/s10858-013-9741-y>
- Vaaje-Kolstad G, Horn SJ, Van Aalten DMF, et al (2005) The non-catalytic chitin-binding protein CBP21 from *Serratia marcescens* is essential for chitin degradation. J Biol Chem 280:28492–28497. <https://doi.org/10.1074/jbc.M504468200>
- Vaaje-Kolstad G, Westereng B, Horn SJ, et al (2010) An oxidative enzyme boosting the enzymatic conversion of recalcitrant polysaccharides. Science (80) 330:219–222.  
<https://doi.org/10.1126/science.1192231>
- Zhang H, Neal S, Wishart DS (2003) RefDB: a database of uniformly referenced protein chemical shifts. J Biomol NMR 25:173–195. <https://doi.org/10.1023/a:1022836027055>